Journal of the Korean Physical Society, Vol. 74, No. 3, February 2019, pp. 245∼250

Experimental and Theoretical Investigation of the Spin Hamiltonian Parameters for the Cr^{3+} Ion in a $BeAl_2O_4$:Cr^{3+} Crystal

Tae Ho Yeom*
Department of Laser and Optical Information Engineering, Cheongju University, Cheongju 28503, Korea

Mao Lu Du
Department of Physics, Southwestern Institute for Nationalities, Chengdu 610041, China and CCAST (World Lab.), Beijing 100080, China

(Received 15 November 2018, in final form 17 December 2018)

The electron paramagnetic resonance of the Cr^{3+} ion in an alexandrite single crystal was explored. The angular dependence of the resonance fields observed using an X-band spectrometer in the crystallographic planes were analyzed using the monoclinic spin Hamiltonian. The spectroscopic splitting tensors g_i and the 2^{nd} order zero field splitting parameters $|D|$ and $|E|$ for the Cr^{3+} center at Al^{3+} site with mirror symmetry (C_s) in an alexandrite crystal were calculated using the crystal field theory for C_s symmetry. Then, the theoretical values were compared with the experimental values. The calculated spin Hamiltonian parameters explain nicely the experimental parameters for the Cr^{3+} center with mirror symmetry.

PACS numbers: 68.43.Bc, 73.20.−r, 75.50.xx
Keywords: $BeAl_2O_4$:Cr^{3+} crystal, EPR, Spin Hamiltonian parameters, Crystal field theory
DOI: 10.3938/jkps.74.245

I. INTRODUCTION

Alexandrite ($BeAl_2O_4$:Cr^{3+}) is a member of the chrysoberyl group of $BeAl_2O_4$. In recent years, it has been proved to be an excellent tunable solid-state laser host with extensive potential applications in scientific, military, and civilian areas [1,2]. Q-switched alexandrite laser has been used in the treatment of bilateral nevus [3]. Synthetic alexandrite is commonly used in medical studies as an active laser material with superior emission characteristics in the 700 nm ∼ 800 nm range [4]. Comprehensive studies examining the medical applications of the alexandrite laser can be found in [5,6]. Also, the potential usage of alexandrite as a dosimetric medium was investigated by means of different methods [7–9].

The space group of $BeAl_2O_4$ crystal is D_{2h}^{16}. Its orthorhombic lattice constants are $a = 0.9404$ nm, $b = 0.5475$ nm, and $c = 0.4427$ nm at room temperature [10]. The unit cell contains four molecules and comprises four beryllium ions at distorted tetrahedral sites and eight aluminum ions at distorted octahedral sites with oxygen ions [11]. However, the substitution of Cr^{3+} for Al^{3+} ions in the host $BeAl_2O_4$ lattice can take place at two physically distinct Al^{3+} sites [11]. This complicates the analysis of the lasing and optical properties [1,12] of this crystal. The two sites both possess distorted octahedral geometry, but one site (Al_1 site) is characterized by inversion symmetry (C_i) and the other (Al_2 site) by mirror symmetry (C_s). Cr^{3+} impurities at each site affect the overall optical properties of the crystal, which is used as laser emitter. Cr^{3+} ions preferably occupy the larger Al_2 site than the smaller Al_1 site [13]. The Cr^{3+} impurity ion at Al_2 site affects the laser properties of alexandrite crystal, whereas the Cr^{3+} impurity ion at Al_1 site do not affect the luminescence spectra, not even helping the laser process [13].

Electron paramagnetic resonance (EPR) is a delicate yet powerful tool when investigating the site location of impurities and their local site symmetry in the host crystal. Magnetic resonance studies of alexandrite single crystal by nuclear magnetic resonance [14–16] and EPR [17,18] have been reported. Crystal field parameter D_q as well as Racah parameters B and C of a red-emitting $BeAl_2O_4$ crystal doped with Mn^{4+} impurity ion are determined. $BeAl_2O_4$: Mn^{4+} single crystal emits intense red light under broad blue light excitation [19,20]. The extensive applications of crystal-field (CF) theory has aided studies on spin-Hamiltonian parameters of $3d^3(^4F)$ ions [21,22]. The theoretical calculations were carried out using the superposition model [23], the lattice relaxation model [24], and the point charge-dipole moment model [25]. These models explore the contributions from different mechanisms to the zero-field splitting (ZFS) and

*E-mail: thyeom@cju.ac.kr

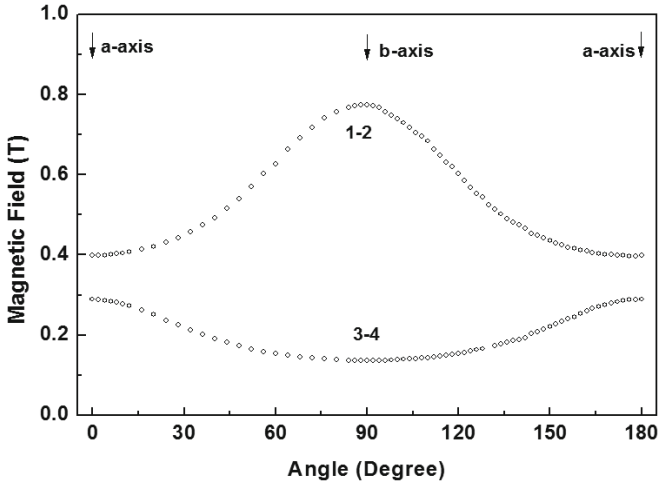

Fig. 1. Angular dependence pattern of EPR fields for the Cr^{3+} ion at Al^{3+} (C_s) site at 9.446 GHz in the *ab*-plane of alexandrite crystal.

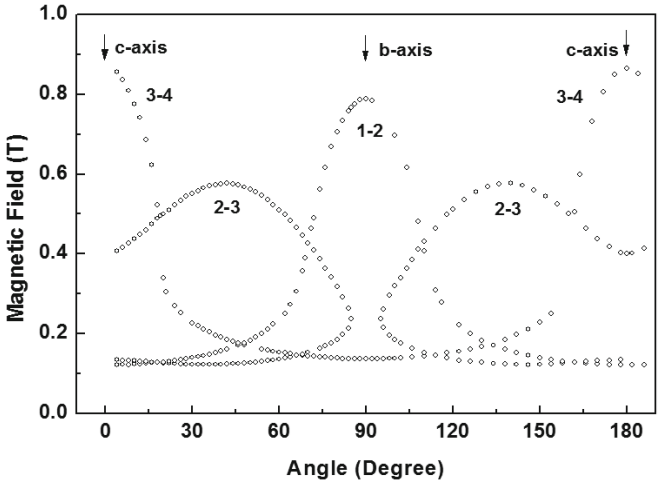

Fig. 2. Angular dependence pattern of EPR fields for the Cr^{3+} ion at Al^{3+} (C_s) site at 9.448 GHz in the *bc*-plane of alexandrite crystal. The levels denoted by 1, 2, 3, and 4 correspond to the quantum states with $M = 3/2$, $1/2$, $-1/2$, and $-3/2$, respectively, for $S = 3/2$ at high field.

give formulae that calculate the ZFS of d^3 ions. The ZFS includes the electrostatic, the crystal-field interaction, and the spin-orbit coupling effects. However, there is no theoretical investigation of the spin Hamiltonian parameters for the Cr^{3+} ion in alexandrite crystal.

In this paper, EPR spectra of Cr^{3+} center at Al_2 site with mirror symmetry in alexandrite single crystal have been analyzed using a monoclinic spin Hamiltonian (SH). The spectroscopic splitting factors and the 2^{nd} order ZFS parameters of Cr^{3+} center at mirror symmetry are computed using the CF theory. The calculated SH parameters agree well with experimental SH parameters. The Cr^{3+} center at inversion site symmetry are not studied here because no theoretical microscopic spin Hamiltonian (MSH) formulae for C_i inversion symmetry are available yet.

II. EXPERIMENTAL ASPECTS

The employed alexandrite single crystal was grown using the Czochralski method by mixing molten Al_2O_3, Cr_2O_3 and BeO powders [26]. The Cr^{3+} impurity ions were doped to 2 mol% concentration in the starting molten mixture. $BeAl_2O_4$:Cr^{3+} strongly tends to grow in a twin structure along <310> directions, resulting in pseudo-hexagonal crystals [17, 27]. This twin structure could lead to multiple EPR resonance lines. However, our alexandrite crystal was found to have no evidence of twining problem judging from the X-ray topography and the nuclear magnetic resonance (NMR) study [16].

The crystallographic directions of the samples were determined using the X-ray Laue method. The EPR measurements were carried out using a Jeol EPR X-band spectrometer (JES-RE2X) at room temperature. The angular dependence of the EPR resonance fields for Cr^{3+} ion with 2° or 4° intervals were measured in the crystallographic planes. There are two chemically inequivalent Cr^{3+} EPR centers which substitute for Al^{3+} ions at C_s and C_i symmetry in alexandrite single crystal [18]. We obtained all resonance fields originated from Cr^{3+} ions at both C_s and C_i symmetry. It turns out that Cr^{3+} centers at C_s symmetry and at C_i symmetry have two and four magnetically equivalent sites, respectively. Only the EPR center originated from Cr^{3+} ion at Al_2 site (C_s symmetry) is discussed in this paper, because no theoretical microscopic spin Hamiltonian formulae for Cr^{3+} ion at Al_1 site (C_i symmetry) are available yet.

The magnetic resonance fields of Cr^{3+} center at Al (C_s) site in crystallographic *ab*- and *bc*-planes were obtained by EPR spectrometer and shown in Fig. 1 and Fig. 2, respectively. The levels denoted by 1, 2, 3, and 4 correspond to the quantum states with $M = 3/2$, $1/2$, $-1/2$, and $-3/2$, respectively, for $S = 3/2$ at high field. The angular dependence of the resonance fields in the *ab*- and *bc*-planes show symmetry. One principal axis of the zero field splitting tensor is found to lie along the *b*-axis for which the angular dependence patterns are symmetrical in the *ab*- and *bc*-planes. This means that the monoclinic direction is parallel to the crystallographic *b*-axis.

III. SPIN HAMILTONIAN ANALYSIS

The Cr^{3+} ($3d^3$) ion has the ground level $^4F_{3/2}$ with $S = 3/2$. When this impurity ion is doped in a crystal, the spin states are affected by the CF produced by the adjacent ions. The experimental EPR resonance field data can be analyzed using the spin Hamiltonian (SH)

Table 1. The measured g_{ij} and D_{ij} values of Cr^{3+} center at Al site with C_s symmetry in alexandrite single crystal.

In the laboratory axis system			In the principal axis system	
	g_{ij}			
1.9711(16)	0	0.0019(9)	g_{XX}	1.9682(9)
	1.9682(9)	0	g_{YY}	1.9687(14)
		1.9704(9)	g_{ZZ}	1.9727(12)
	D_{ij}/h (MHz)			
−701(2)	0	308(2)	D_{XX}	−718(2)
	−4179(2)	0	D_{YY}	−4179(2)
		4880(2)	D_{ZZ}	4897(2)

in the conventional notation [28,29].

$$H = H_{\rm Ze} + H_{\rm ZFS} = \mu_{\rm B}\vec{B}\cdot\overleftrightarrow{g}\cdot\vec{S} + \vec{S}\cdot\overleftrightarrow{D}\cdot\vec{S}, \quad (1)$$

where $\mu_{\rm B}$ denotes the Bohr magneton, $\vec{B}$ the applied magnetic field, $\overleftrightarrow{g}$ the spectroscopic splitting tensor, $\vec{S}$ the electron spin operator, and $\overleftrightarrow{D}$ the zero-field splitting (ZFS) tensor. The monoclinic spin Hamiltonian of ZFS interaction for our crystal system (monoclinic axis // crystallographic b-axis) can be expressed in the 'Extended Stevense parameters' as follows [29,30]:

$$H_{\rm ZFS}^{\rm momo} = B_k^q O_k^q = B_2^0 O_2^0 + B_2^1 O_2^1 + B_2^2 O_2^2. \quad (2)$$

The "laboratory" axes system used for the SH analysis are denoted by x, y, z, and are chosen to lie on the crystallographic axes a, b, and c, respectively. The software (EPR version 6.0) utilized here builds the spin-Hamiltonian matrices and computes their eigenvalues by means of diagonalization [31]. The input parameters are optimized through nonlinear least-squares routines in order to minimize the discrepancies between the calculated and observed transition frequencies along with the magnetic resonance fields. A sum of 542 resonance line positions obtained in the crystallographic planes due to the ZFS of Cr^{3+} in alexandrite are used for fitting using the monoclinic SH in Eq. (1). The final best-fit constants $\overleftrightarrow{g}$ and $\overleftrightarrow{D}$ computed by EPR version 6.0 are presented in Table 1. The approximated statistical uncertainties in the last significant figure are shown in the parentheses. The sum of the final root mean squares of the discrepancies between the calculated and observed figures is 63 MHz for the resonance frequencies and 2.2 mT for the EPR fields. The values of g_{ij} and D_{ij} imply that the local site symmetry of Cr^{3+} ion at Al^{3+} site with mirror symmetry in alexandrite crystal is monoclinic. The D_{ij} in Table 1 are related to the conventional ZFS D and E parameters as follows [29]:

$$D = \frac{3}{2}D_{ZZ}, \quad E = \frac{1}{2}(D_{XX} - D_{YY}). \quad (3)$$

The energy levels of Cr^{3+} at the C_s symmetry site (Al_2 site) in alexandrite crystal as a function of the external magnetic field applied parallel to the crystallographic

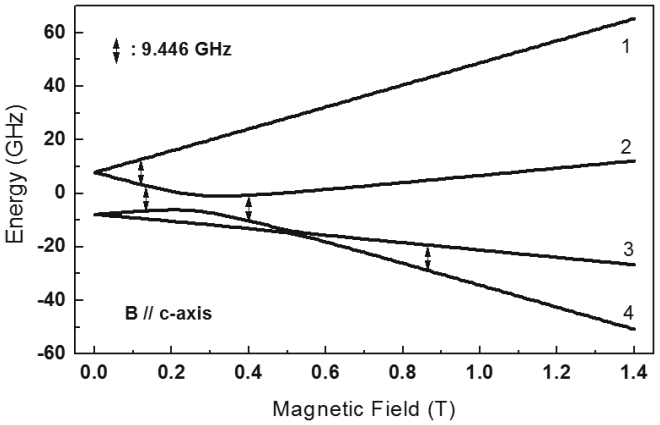

Fig. 3. The energy levels of Cr^{3+} in alexandrite single crystal as a function of the external magnetic field applied parallel to the crystallographic c-axis.

c-axis are computed using optimized spin Hamiltonian parameters as shown in Fig. 3. The arrows show the observed transition at 9.446 GHz. The resonance fields 0.1200, 0.1331, 0.4007, and 0.8647 T indicated with arrows in Fig. 3 correspond to the experimental resonance fields when **B** // the crystallographic c-axis in Fig. 2. The levels denoted by 1, 2, 3, and 4 correspond to the quantum states with $M = 3/2$, $1/2$, $-1/2$, and $-3/2$, respectively, for $S = 3/2$ at high field. The energy splitting at $B = 0$, *i.e.* the ZFS, arising from the CF, spin-orbit interaction, and spin-spin interaction, is measured as 0.529 cm^{-1}.

IV. MICROSCOPIC SPIN HAMILTONIAN CALCULATIONS

The ZFS depends sensitively on the local structure, particularly, the bond angles as well as the bond lengths, in the vicinity of the paramagnetic ion. In this section, the g values and the 2^{nd} order ZFS parameters (D and E) of Cr^{3+} ion sitting at the Al_2 (C_s) site in alexandrite crystal are computed using the 3rd order perturbation formulae [25]. For the C_2 symmetry system, the perturbation formulae of the g-tensor and the ZFS constants (D and E) of d^3 ion have been derived [25]. The crystal structure and symmetry sites of the Al^{3+} ions which are replaced by Cr^{3+} impurity ions in the alexandrite crystal are well described in several references [11,27,32, 33]. Since the crystal field Hamiltonian of C_s symmetry system is the same as that of C_2 symmetry system [34], the third-order perturbation formulae of C_2 symmetry for the EPR constants g, D, and E can be used with

those of C_s symmetry as follows:

$$\begin{aligned} g_z =& g_e - \frac{8\zeta_d}{3D_1} - \frac{2\zeta_d^2}{27D_1^2}(2g_e+1) - \frac{4\zeta_d^2}{9D_1D_2} \\ & - \frac{2\zeta_d^2}{9D_2^2}(g_e+1) + \frac{4\zeta_d^2}{9D_2D_3} - \frac{4\zeta_d^2}{27D_3^2}(2g_e-1) \\ & + \frac{4\zeta_d^2}{27D_3D_1} + \frac{16\zeta_d}{9D_1^2}D_\eta \end{aligned} \tag{4a}$$

$$g_x = g_z - \frac{2\zeta_d}{9D_1^2}(35D_t + 7D_\eta + 7D_\xi) \tag{4b}$$

$$g_y = g_z - \frac{2\zeta_d}{9D_1^2}(35D_t + 7D_\eta - 7D_\xi) \tag{4c}$$

And

$$D = \frac{35\zeta_d^2}{9D_1^2}D_t - \frac{35\zeta_d^2}{9D_3^2}D_t + \frac{7\zeta_d^2}{9D_1^2}D_\eta - \frac{7\zeta_d^2}{9D_3^2}D_\eta \tag{5a}$$

$$E = \frac{7\zeta_d^2}{9D_1^2}D_\xi + \frac{7\zeta_d^2}{9D_3^2}D_\xi \tag{5b}$$

where, ζ_d denotes the spin-orbit coupling coefficient, D_q, D_t, D_η, and D_ξ denote the crystal-field parameters, and $g_e = 2.0023$ is the spin only g-value. The energy denominators can be obtained from optical data as follows:

$$D_1 = W(^4T_2) - W(^4A_2) \tag{6a}$$

$$D_2 = W(^2T_2) - W(^4A_2) \tag{6b}$$

$$D_3 = W(^2T_2) - W(^4A_2). \tag{6c}$$

Because the crystallographic ac-plane (xz-plane) is the mirror plane as follows from the crystallographic data (see Fig. 1 in Ref. 11), the crystal field parameters for the Cr^{3+}-center at mirror symmetry in $BeAl_2O_4$ crystal are derived using the point-charge dipole moment model as follows:

$$D_q = -\frac{1}{6}\frac{eq<r^4>}{\bar{R}^5}\left(1+\frac{5\mu}{qR}\right) \tag{7a}$$

$$\begin{aligned} D_t =& \frac{1}{3}eq<r^4>\left(1+\frac{5\mu}{qR}\right) \\ & \times\left[\frac{1}{56}\left\{\frac{1}{R_1^5}(35\cos^4\theta_1 - 30\cos^2\theta_1 + 3)\right.\right. \\ & + \frac{2}{R_3^5}(35\cos^4\theta_3 - 30\cos^2\theta_3 + 3) \\ & + \frac{1}{R_2^5}(35\cos^4\theta_2 - 30\cos^2\theta_2 + 3) \\ & \left.\left. + \frac{2}{R_4^5}(35\cos^4\theta_4 - 30\cos^2\theta_4 + 3)\right\}\right. \\ & \left. + \frac{1}{3}\frac{1}{\bar{R}^5}\right] \end{aligned} \tag{7b}$$

$$\begin{aligned} D_\xi =& \frac{5}{42}eq<r^4>\left(1+\frac{5}{\mu/qR}\right) \\ & \times\left\{\frac{1}{R_1^5}(7\cos^2\theta_1 - 1)\sin^2\theta_1\right. \\ & + \frac{2}{R_3^5}(7\cos^2\theta_3 - 1)\sin^2\theta_3\cos 2\varphi_3 \\ & + \frac{1}{R_2^5}(7\cos^2\theta_1 - 1)\sin^2\theta_2 \\ & \left. + \frac{2}{R_4^5}(7\cos^2\theta_4 - 1)\sin^2\theta_4\cos 2\varphi_4\right\} \end{aligned} \tag{7c}$$

$$\begin{aligned} D_\eta =& -\frac{5}{24}eq<r^4>\left(1+\frac{5\mu}{qR}\right) \\ & \times\left(\frac{1}{R_1^5}\sin^4\theta_1 + \frac{2}{R_3^5}\sin^4\theta_3\cos 3\varphi_3\right. \\ & \left. + \frac{1}{R_2^5}\sin^4\theta_2 + \frac{2}{R_4^5}\sin^4\theta_4\cos 4\varphi_4\right) \end{aligned} \tag{7d}$$

where R_i and $\bar{R}$ are the bond lengthes and average bond length of Cr^{3+}-O^{2-} ligand, respectively; θ_i and φ_i the bond angles of Cr^{3+}-O^{2-}, e electronic charge, q ligand charge, $<r^4>$ expectation value of Cr^{3+} ion, μ the electric dipole moment of ligand. The CF parameters $(D_q, D_t, D_\eta, D_\xi)$ in Eq. (7) derived for the 6-fold coordination with C_s symmetry differ from those for the C_2 symmetry in Ref. 25.

Zhao proposed a parameterization d-orbit method [35, 36], which can be used in the calculation of the d-d crystal field transition, the ZFS, and the g factors, using the structural data. These orbitals have successfully interpreted the optical and magnetic properties of the transition metal clusters. According to the average covalent factor model [37], the Racah electrostatic parameters (B_0 and C_0), the expectation value $<r^4>$, and the spin-orbit coupling coefficient ζ_d in crystal can be obtained as

$$B = N^4B_0, C = N^4C_0 \tag{8a}$$

$$<r^4> = N2<r^4>_0 \tag{8b}$$

$$\zeta_d = N^2\zeta_d^0 \tag{8c}$$

where $<r^4>_0$ and ζ_d^0 denote the values of the free ion and N the average covalency parameter. The values B_0, C_0, $<r^4>_0$, and ζ_d^0 are obtained by parameterization of d-orbit for Cr^{3+} ion in Ref. 37 as follows:

$$<r^4>_0 = 16.4276 \text{ a.u.}, \quad \zeta_d^0 = 242 \text{ cm}^{-1}$$

$$B_0 = 920.48 \text{ cm}^{-1}, \quad C_0 = 3330.71 \text{ cm}^{-1}.$$

The energy matrix of d^3 in cubic field [38] is determined by the Racah electrostatic parameters B, C, and cubic crystal field parameter D_q. Using the above values B_0, C_0, $<r^4>_0$, and ζ_d^0, one can obtain the values D_q, B, and C from Eq. (7.1) and (8.1). Taking N and μ as fitting parameters and using the crystal structure data, the d-d transitions of Cr^{3+} ion in $BeAl_2O_4$ crystal with cubic field approximation can be calculated by diagonalization of the matrix. The calculated values are listed

Table 2. The d-d transitions for Cr^{3+} center at Al site with C_s symmetry in $BeAl_2O_4$:Cr^{3+} crystal.

Transition		Calculated (cm^{-1})	Experimental (cm^{-1})	
			Ref. 35	Ref. 26
$^4A_2 \rightarrow$	$^2E(G)$	14751	14071, 14747	14741
	$^2T_1(G)$	15527	$\sim$ 15300	15290, 15533
	$^4T_2(F)$	18194	16650, 16750, 18320	17643
	$^2T_2(D2)$	22271	$\sim$ 21400	20408
	$^4T_1(F)$	26096	23000, 13700, 24230	24284
	$^2A_1(G)$	30299		32616
	$^2T_2(G)$	32840		37821
	$^2T_1(P)$	33367		

Table 3. The bond lengthes and bond angles (θ_i, φ_i) for Cr-O_i, Cr^{3+} ion residing at the Al site with mirror symmetry in $BeAl_2O_4$:Cr^{3+} single crystal.

	Cr-O_1	Cr-O_2	Cr-O_3	Cr-O_4
R (nm)	0.1862	0.1940	0.2017	0.1895
θ (degree)	55.16	116.52	53.31	124.62
φ (degree)	0	180	129.06	67.77

and compared to those of the experiments [26,39] in Table 2. The values of the average factor N and the dipole moment μ are determined as $N = 0.97$ and $\mu/eR = 0.12$, respectively.

From the structural data of $BeAl_2O_4$ [11,40], the bond lengthes R_i and bond angles θ_i, φ_i for Cr^{3+} at Al_2 (C_s) site are obtained as shown in Table 3. Here the bond lengths and angles of Cr-O_i bonds in Table 3 are assumed to be the same as those of Al-O_i bonds at C_s symmetry. Then, the crystal field parameters D_q, D_t, D_ξ, and D_η of Cr^{3+} ion were calculated from the structural data in Table 3 and the values of $N = 0.97$ and $\mu/eR = 0.12$ calculated from the d-d transition. The spin Hamiltonian parameters g_i, D and E for Cr^{3+} at the Al_2 (C_s) site in alexandrite are obtained using Eqs. (4) and (5) in the laboratory axis system. In the above calculation, experimental energy level $D_1 = 16750$, $D_2 = 21400$, and $D_3 = 37821$ cm^{-1} [26,39] are used. The spin Hamiltonian parameters calculated in the laboratory axis system are presented in Table 4 (Set A). The empirical data of the ZFS parameters (D_{ij}) in Table 1 were converted into D and E in Table 4 (Set B) in order to compare with the microscopic spin Hamiltonian calculation as well as other experimental data [17,18]. The monoclinic terms g_{xz} (= 0.0019) and D_{xz} (= 0.0103 cm^{-1}) in Table 1 are not shown in Table 4 (Set B) because the other data [17,18] do not have monoclinic terms and the monoclinic terms are not substantial.

The experimental values D and E obtained in the laboratory axis system with orthorhombic symmetry of Cr^{3+} are shown in Set C (Ref. 17) and Set D (Ref. 18) in Table 4 for comparison. The sign of ZFS parameters are not determined here and only absolute values

Table 4. Calculated spin Hamiltonian parameters for Cr^{3+} ion at the Al site with C_s symmetry in the laboratory axis system of $BeAl_2O_4$:Cr^{3+} crystal. The absolute values of D and E for the set A and B are only determined.

	Calculation	Experiment		
	(present work)	(present work)	Ref. 17	Ref. 18
	[Set A]	[Set B]	[Set C]	[Set D]
g_x	1.966	1.9711	1.978	1.9789
g_y	1.967	1.9682	1.980	1.9804
g_z	1.968	1.9704	1.969	1.9789
$\lvert D\rvert$ (cm^{-1})	0.2168	0.2450	0.2438	0.2446
$\lvert E\rvert$ (cm^{-1})	0.0367	0.0577	0.0570	0.0580

of D and E are considered in Table 4. The calculated 2^{nd} order ZFS parameters $|D|$ (= 0.2168 cm^{-1}) and $|E|$ (= 0.0367 cm^{-1}) in Set A reasonably fit the empirical values $|D|$ (= 0.2442 cm^{-1}) and $|E|$ (= 0.0580 cm^{-1}) in Set B. It reveals that the ZFS is mainly originated from the CF and spin-orbit interaction. The ZFS difference between the calculated and experimental parameters may originate from the orthorhombic approximation of crystal field Hamiltonian. The theoretical values of g-factors are also congruent with the experimental values.

Barry and Troup [17] determined the spin Hamiltonian parameters of Cr^{3+} at Al^{3+} site with mirror symmetry using the orthorhombic spin Hamiltonian as shown in Table 4 (Set C). The correlation between the crystallographic and magnetic axes slightly deviates from the crystallography of pure chrysoberyl [17]. The ZFS parameters in Set C determined by using the orthorhombic spin Hamiltonian are not much different from those in Set B determined by using the monoclinic spin Hamiltonian. It means that the monoclinicity of Cr^{3+}-center at Al^{3+} site with mirror symmetry is small. The rotation patterns in Figs. 1 and 2 as well as the spin Hamiltonian parameters in Table 1 for Cr^{3+} at the Al^{3+} (C_s) site indicate that the local site symmetry of Cr^{3+}-center is monoclinic even though monoclinicity is not substantial. Forbs [18] also obtained the spin Hamiltonian parameters with orthorhombic symmetry for Cr^{3+} at mirror site as shown in Table 4 (Set D). The values $|D|$ and $|E|$ in Set D are also similar with those in Set C as well as our experimental values in Set B.

V. CONCLUSION

The rotation patterns of Cr^{3+} ion in alexandrite crystal, grown using the Czochralski method, are examined in the crystallographic planes at room temperature. The spin Hamiltonian parameters of the Cr^{3+} centers substituted in Al^{3+} sites at mirror symmetry in an alexandrite single crystal were determined using the monoclinic spin Hamiltonian. The monoclinic direction turned out to

be parallel to the crystallographic direction b-axis. The spectroscopic splitting parameters g_i and the 2^{nd} order ZFS parameters D and E were computed using the CF theory and compared with experimental parameters. The microscopic spin Hamiltonian theory explains well the experimental parameters. Our results have been analyzed to derive the substitutional site as well as actual local site symmetry of the Cr^{3+} ion from the experimental and theoretical calculations. Cr^{3+} impurities at each Al site, at C_s symmetry and C_i symmetry, in alexandrite single crystal are responsible for the overall optical properties of the crystal, which is used as the laser emitter. The analysis of Cr^{3+} impurity ion which plays an important role in lasers is very helpful in the enhancement of the lasing and optical properties of the alexandrite crystal.

REFERENCES

[1] J. C. Walling, O.G. Peterson, H. P. Jenssen, R. C. Morris and E. W. O'Dell, IEEE J. Quantum Electron. **QE-16**, 1302 (1980).
[2] J. C. Walling, Laser Focus **1**, 45 (1982).
[3] W. Yu, J. Zhu, W. Yu, D. Lyu, X. Lin and Z. Zhang, J. Am. Acad. Dermatol. **79**, 479 (2018).
[4] R. M. F. Scalvi, M. S. Li and L. V. A. Scalvi, Phys. Chem. Miner. **31**, 733 (2005).
[5] N. Saedi, A. Metelitsa, K. Petrell, K. A. Arndt and J. S. Dover, Arch. Dermatol. **148**, 1360 (2012).
[6] Y. K. Kim, D. Y. Kim, S. J. Lee, W. S. Chung and S. B. Cho, J. Eur. Acad. Dermatol. Venereol. **28**, 1007 (2014).
[7] N. M. Trindade, H. Kahn and E. M. Yoshimura, J. Lumin. **195**, 356 (2018).
[8] N. M. Trindade, A. L. M. C. Malthez, A. de C. Nascimento, R. S da Silva, L. G. Jacobsohn and E. M. Yoshimura, Optical Materials **85**, 281 (2018).
[9] E. Grillo, P. Gonzalez-Munoz, P. Boixeda, A. Cuevas, S. Vano and P. Jaen, Actas Dermosifiliogr. **107**, 591 (2016)
[10] H. E. Swanson M. I. Cook, T. Issacs and E. H. Evans, Natl. Bur. Std. Circ. **539**, 10 (1960).
[11] E. F. Farrell, J. H. Fang and R. E. Newnham, Amer. Mineralogist **48**, 804 (1963).
[12] M. L. Shand and H. P. Jenssen, IEEE J. Quantum Electron. **QE-19**, 480 (1983).
[13] D. A. Vinnik, D. A. Zherebtsov, S. A. Archugov, M. Bischoff and R. Niewa, Cryst. Grow. Des. **12**, 3954 (2012).
[14] T. H. Yeom, A. R. Lim, S. H. Choh, K. S. Hong and Y. M. Yu, J. Phys.: Condens. Matter **7**, 6117 (1995).
[15] T. H. Yeom, K. S. Hong, I. Yu, H. W. Shin and S. H. Choh, J. Appl. Phys. **82**, 2472 (1997).
[16] T. H. Yeom and S. H. Choh, J. Korean Phys. Soc. **45**, 1606 (2004).
[17] W. R. Barry and G. J. Troup, phys. stat. sol. **35**, 861 (1969).
[18] C. E. Forbes, J. Chem. Phys. **79**, 2590 (1983).
[19] J. Hu, Y. Zhao, B. Chen, H. Xia, Y. Zhang and H. Ye, Ceramics International **44**, 20220 (2018).
[20] S. Ghanbari and A. Major, Laser Phys. **26**, 075001 (2016).
[21] Y. Y. Yeung and D. J. Newman, Phys. Rev. B **34**, 2258 (1986).
[22] M. L. Du and M. G. Zhao, Solid State Commun. **76**, 565 (1990).
[23] D. J. Newman, J. Phys. C: Solid State Phys. **15**, 6627 (1982).
[24] Y. Y. Yeung, J. Phys.: Condens. Matter **2**, 2461 (1990).
[25] X. P. He and M. L. Du, J. Phys. Chem. Solids **49**, 339 (1988).
[26] R. H. Bak, Y. M. Yu and Y. K. Lee, Korean Crystallogr. **3**, 111 (1992).
[27] P. P. Phakey, phys. stat. sol. **32**, 801 (1969).
[28] A. Abragam and B. Bleaney, *Electron Paramagnetic Resonance of Transition Ions* (Oxford University Press, Oxford, 1970), Chaps. 3 and 7.
[29] C. Rudowicz, Mag. Res. Rev. **13**, 1 (1987).
[30] S. K. Misra and C. Rusowicz, phys. stat. sol. (b) **147**, 677 (1988).
[31] M. J. Mombourquette, J. A. Weil and D. G. McGavin, *Operating Instruction for Computer Program EPR-NMR ver. 6.0* (Univ. of Saskatchewan, Canada, 1995).
[32] J. H. Hockenberry, L. C. Brown and D. Williams, J. Chem. Phys. **28**, 367 (1958).
[33] H. L. Reaves and T. E. Gilmer, J. Chem. Phys. **42**, 4138 (1965).
[34] C. Rusowicz, J. Chem. Phys. **84**, 5045 (1986).
[35] M. G. Zhao and M. L. Du, Phys. Rev. B **28**, 6481, (1983).
[36] M. G. Zhao, M. L. Du and G. Y. Sen, J. Phys. C **20**, 5557 (1987).
[37] M. G. Zhao, J. A. Xu, G. R. Bai and H. S. Xie, Phys. Rev. B **27**, 1516 (1983).
[38] J. S. Griffith, *The Theory of Transition-Metal Ions* (Cambridge University Press, 1961).
[39] G. Z. Wu and X. R. Zhang, Acta Physics Sinica **32**, 64 (1983)
[40] X. S. Ma, J. J. Lu and Z. Y. Qian, Acta Phys. Sinica **32**, 1302 (1983).